Available online at www.sciencedirect.com
SCIENCE DIRECT®
Cement & Concrete Composites 26 (2004) 935–945
Cement & Concrete Composites
www.elsevier.com/locate/cemconcomp

Backscattered electron imaging of cementitious microstructures: understanding and quantification

Karen L. Scrivener *

Laboratory of Construction materials, IMX, Ecole Polytechnique Fédérale de Lausanne, 1015 Lausanne, Switzerland

Abstract

During the last 20 years, backscattered electron imaging of polished surfaces has become well established as a method for the study of cement and concrete microstructures. The technique has many advantages, including the visualisation of representative cross-sections over a wide range of magnifications and reproducible contrast dependent on atomic number. Nevertheless the limitations of observing a two-dimensional section of a three-dimensional structure must be borne in mind.

In this paper, the general microstructural features of hydrated cement pastes are described. Although the amount of aluminate phase (''C_3A'') in cement is comparatively minor, it plays an important role in determining many of the microstructural features of cement paste microstructure, for example in the formation of ''Hadley'' grains.

Despite the very heterogeneous nature of cement paste, it is important to be able to derive quantitative measures if the relationships between microstructure and properties are to be understood. The possibilities to quantify BSE images are described. The interface between paste and aggregates in concrete is particularly variable, but average features can be measured, which help to understand the processes of packing cement grains, which gives rise to this region. Finally an example of the potential for BSE images to study concrete durability is given.

Keywords: Microstructure; Scanning electron microscopy (SEM); Hardened cement paste (HCP); C–S–H gel; Pore structure; Interfacial transition zone (ITZ)

1. Introduction

Since its first use in the early 1980s [1,2], backscattered electron (BSE) imaging has demonstrated its great potential for the study of cementitious materials. The advantages of this technique are:

- Observation of flat polished sections, which can be prepared to be representative (compared to fracture surfaces that reveal a path of weakness).
- Wide range of magnifications from about 20× to 10,000× so that features can be seen in detail and in context (compared to TEM where relatively small areas are observed, or fracture surfaces where only a crack path is visible). At low magnifications, the arrangement of aggregates, paste and any defects in a concrete may be studied. At the highest magnifications, it is possible to observe the morphology of the hydrate phases — C–S–H, ettringite, etc. and pores down to about 100 nm.
- Reproducible contrast which allows quantification by image analysis of the different microstructural constituents.
- Possibility to combine BSE imaging with information from local chemical microanalyses.

The main limitations of the technique are spatial resolution, which is less than secondary electron imaging (used with fracture surfaces) and the fact that only two-dimensional sections of a three-dimensional microstructure may be observed. Although the later point is common to all microscopical techniques, the consequences are not usually well appreciated. As illustrated in Fig. 1, the most important of these consequences are:

(a) The section, through cement grains, aggregates, etc., will generally not be equatorial, so the thickness of features such as layers will be overestimated.
(b) The particle size distribution observed will be skewed towards smaller particles by the same sectioning

* Tel.: +41-21-693-5843; fax: +41-21-693-5800.
E-mail address: karen.scrivener@epfl.ch (K.L. Scrivener).

0958-9465/$ - see front matter © 2004 Elsevier Ltd. All rights reserved.
doi:10.1016/j.cemconcomp.2004.02.029

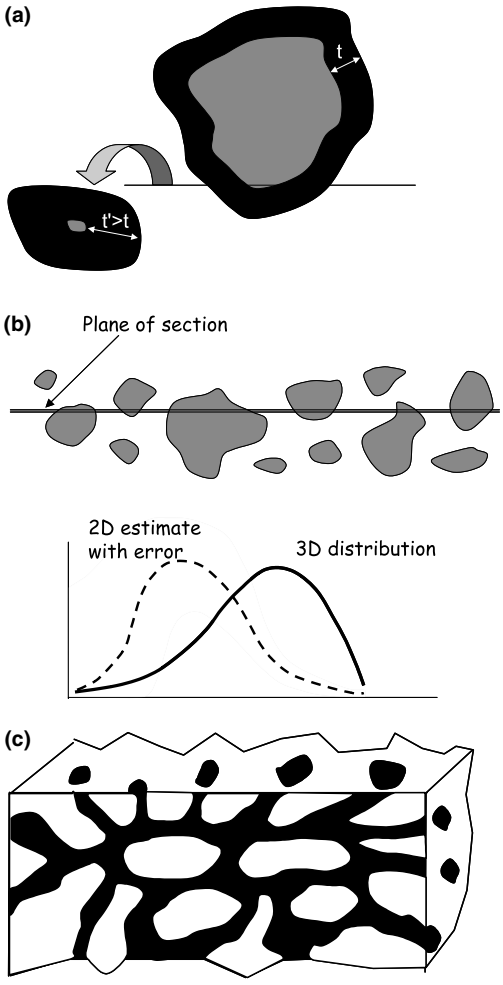

Fig. 1. BSE images give a two-dimensional image of a three-dimensional microstructure. This figure illustrates three consequences of this: (a) The section will rarely pass equatorially through a particle. Therefore the thickness of layers surrounding particles will tend to be exaggerated. (b) For a distribution of particles the size distribution in 2D will be skewed towards smaller particles which are sections of larger particles in 3D. In addition, small particles are cut more rarely so the error in the determination of the number of small particles is very high. (c) Pores which appear unconnected on a 2D section, may in fact be connected in 3 dimensions.

effect described above. Methods for transforming two-dimensional size distributions to three-dimensional ones only exist for simple, convex shapes. As small particles have less chance of being sectioned than large ones, the error in the estimation of the number of small particles is very large.

(c) Connectivity of a 3-D structure cannot be deduced from 2-D sections.

This paper reviews some of the features of cement and concrete microstructures which have been studied with the use of backscattered electrons, with discussion of the possibilities for quantification. Throughout the text the expression ''cement pastes'' should be taken also to include the paste portion of mortars and concretes.

2. Physics of BSE imaging and X-ray microanalysis

Backscattered electrons are electrons from the incident beam which are scattered through large angles so that they re-emerge from the specimen. They have higher energy than secondary electrons and so are detected from greater depths (Fig. 2). This is responsible for the lower resolution of BSE images compared to secondary electron images. The intensity of the BSE signal is mainly a function of the average atomic number of the local area of the sample. With flat polished sections and coupled detectors on either side of the beam, topographic contrast is effectively eliminated. It is this reproducible contrast which makes BSE imaging such a valuable technique. The incorporation of water during hydration leads to hydrates which have much lower average atomic numbers than the anhydrous materials, and thus strong contrast is obtained between unreacted (anhydrous) and reacted material (hydrates). There is weaker, but still discernable, contrast between the anhydrous phases, with Ferrite solid solution being noticeably brightest followed by alite (C_3S) and then by aluminate (C_3A) and belite (C_2S) which are very similar in grey level. Within the hydrates, Portlandite (CH) is significantly brighter than the other hydrates. However, it is not possible to differentiate on the basis of grey level alone between the other hydrates (C–S–H, ettringite, AFm phase, etc.).

X-rays are generated throughout the interaction volume shown in Fig. 2. Typically for cementitious materials this volume is around 1–2 μm across. This is larger than the size of many hydrate phases, so analyses will typically come from mixtures of phases. The characteristic X-rays can be analysed by energy dispersive or wavelength dispersive detectors to give the chemical composition of the local area. The most commonly used

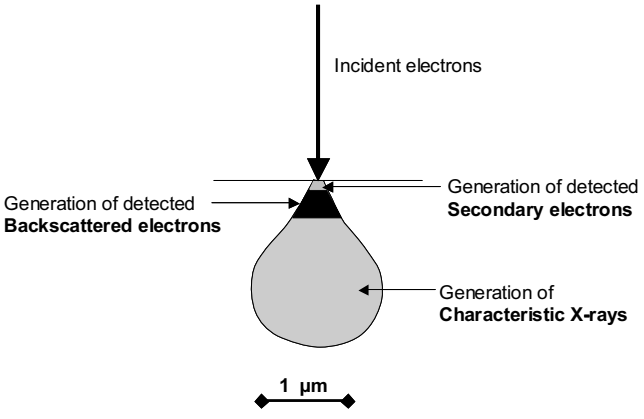

Fig. 2. Signal generation in the scanning electron microscope (SEM). Secondary electrons are detected from close to the surface, electrons are backscattered from a somewhat greater depth and characteristic X-rays are generated throughout the interaction volume of the electrons with the specimen.

technique, energy dispersive spectroscopy (EDS), has an accuracy and detection limit of around 1%.

3. Origins of microstructure in cementitious materials

The microstructure of cementitious materials develops by hydration. In the hydration reaction, the anhydrous cement grains react with water to produce hydrates, and in the process increase the solid volume of the system. This additional solid bridges the spaces between grains, leading to the formation of a solid mass. In Portland cement paste, the hydration reaction is dominated by the reaction of the tri calcium silicate (C_3S), which produces calcium hydroxide (CH) and calcium silicate hydrate (C–S–H). The deposition of these phases in the microstructure is quite distinct—CH precipitates in the water filled pores, while C–S–H deposits mainly around the cement grains. This broad scheme of microstructural formation enables the essential features of BSE images, such as Fig. 3 to be interpreted.

4. Impact of clinker mineralogy

The simple scheme described above is complicated by the fact that Portland cement does not consist only of C_3S. The clinker contains four main phases—impure C_3S (alite), impure C_2S (belite), impure C_3A (aluminate) and impure $Ca_2(Al,Fe)$ (Ferrite solid solution, Fss). During grinding, facture generally occurs through the phases rather than between them, so that the resulting cement grains almost always contain more than one phase.

The effect of the polymineralic nature of the cement grains and the different rates of reactivity of the clinker phases can be seen in mature cement pastes. Some examples are shown in Fig. 4. The central grain in Fig. 4(a) consists mainly of alite, which has reacted fairly evenly to give a layer of C–S–H about 6 μm thick around the unreacted core. At the top of this grain is a large area

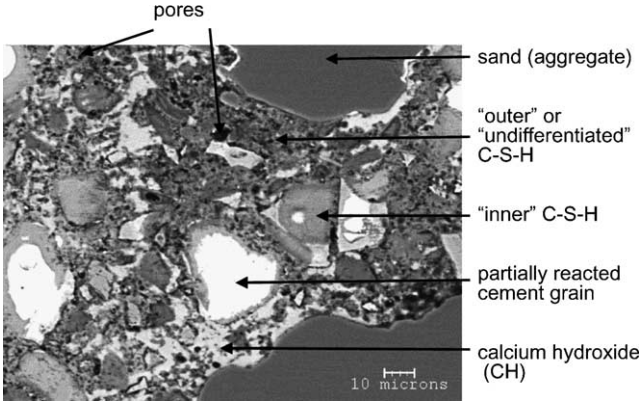

Fig. 3. Typical BSE image of a Portland cement mortar (200 days old, $w/c = 0.4$), with the microstructural constituents distinguished.

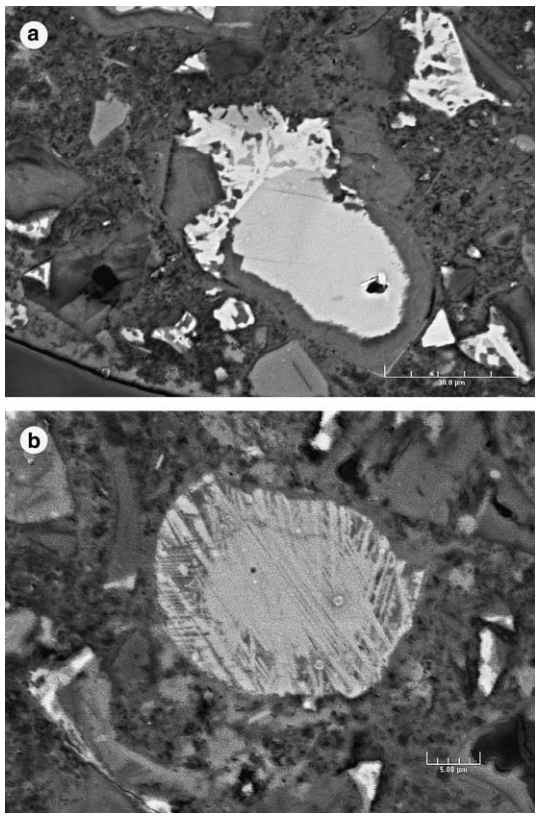

Fig. 4. BSE images of different cement grain partially hydrated (28 days). (a) Grain containing mainly alite, which has reacted fairly evenly with a large mass of interstitial materials (aluminate + ferrite) to the upper left. The bright ferrite appears little reacted and has shielded the reactive aluminate phase, which remains unhydrated at the centre of the mass. (b) Belite grain, showing preferential reaction along striations, probably due to the different solute content of the striations.

of interstitial material (Fss plus aluminate). The Fss appears not to have reacted at all maintaining its original outline. Much of the aluminate phase has reacted, but in the centre of the interstitial region, where it is protected by the Fss and alite, anhydrous C_3A remains.

The central grain in Fig. 4(b) consists of belite, the characteristic striations arise from crystal twinning produced during cooling of the clinker. Due to the fractionation of solutes, the striations react at different rates to a maximum depth of about 4 μm.

Perhaps the most significant impact of the polymineralic nature of cement grains is in the formation of ''separated hydration shells''. This effect can be seen by comparing Fig. 5(a) and (b). In both cases the starting material was 70% C_3S, 10% C_2S, 10% C_3A, 10% Fss with the addition of 5% gypsum, hydrated for 3 days. In case (a) these were mono-mineralic powders of the different phases mechanically mixed together, whereas case (b) was a ground clinker with poly-mineralic grains. In case (a) a fairly even rim of C–S–H can be seen around each C_3S grain, while the matrix is filled with a fine mixture of hydrates including C–S–H and calcium alumino monosulfate. In case (b), the larger grains are

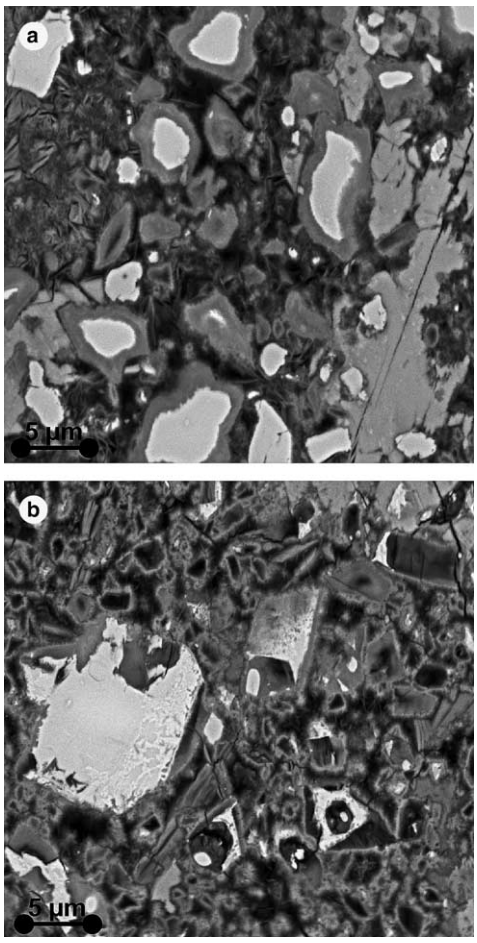

Fig. 5. Effect of clinker microstructure (both hydrated for 7 days at $w/c = 0.5$). (a) Shows a hydrated mixture of clinker phases—monomineralic grains of C_3S, C_3A and C_2S. The C_3S grains are immediately surrounded by hydration products, while the aluminate phase has completely reacted give calcium monosulfoaluminate (b) shows a clinker in which the grains are polymineralic. In this case the formation of separated hydration shells (Hadley grains) is much more obvious and the main calcium sulfo aluminate phase present is ettringite.

surrounded by a thin shell of C–S–H, which is separated from the partially reacted cores by a gap of around 1 μm. The reasons for this phenomenon are not well understood, but the aluminate phase clearly has an important influence. Studies of the hydration of C_3A with gypsum in an environmental cell in a high voltage transmission electron microscope, showed the development of an ill-defined, probably amorphous, product on the surface of the grains within the first 10 min together with ettringite forming at some distance from the grains (Fig. 6). The formation of this possibly amorphous product on the surface of the Portland cement grains might inhibit the precipitation of C–S–H on the grain surface and lead to the formation of the separated shells that have been observed.

This hydrate shell forms between the end of the induction period and about 1 day. Grains smaller than about 5 μm in size hydrate completely during this stage to

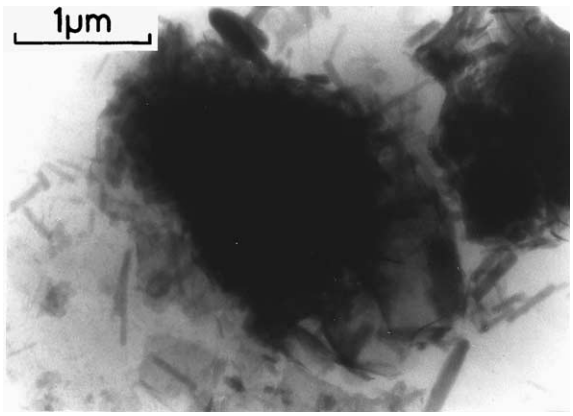

Fig. 6. C_3A hydrated in the presence of gypsum after 10 min in an environmental cell of a high voltage transmission electron microscope. In the solution ettringite needles can be seen, but there is also a dense mass of material of ill defined morphology (perhaps amorphous) surrounding the reacting grain.

leave hollow hydration shells—so-called Hadley grains. These are a common feature in all cement pastes, even those mixed at very low water to cement ratios. Although the pores inside Hadley grains are several microns in size, they are isolated so their size is not reflected by commonly used measurement techniques, such as mercury intrusion porosimetry. Larger grains continue to hydrate and more dense C–S–H forms on the inside to the shells, so that the gap disappears after about 7–14 days.

Fig. 7 shows schematically how grains of different sizes hydrate. The smallest grains (less than about 5 μm)

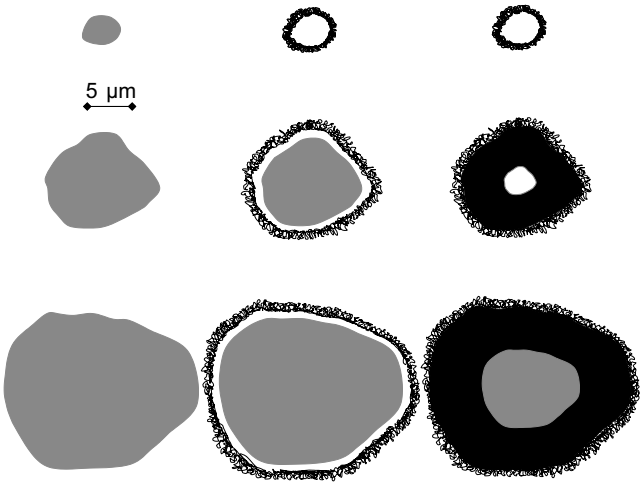

Fig. 7. Schematic illustration of the formation of separated hydration shells over time according to grain size. The middle column shows the situation after about one day, all grains are surrounded by a thin shell of C–S–H separated by around 1 μm from the underlying grain. The column on the right shows the situation in the mature paste. Small grains (top) hydrate completely in the first stage and remain as hollow shells of hydration product. Medium size grains (middle) form a thicker rim of C–S–H as the grain continues to hydrate, perhaps with a small hole at the centre. Grains larger than about 15 μm hydrate to fill in the gap between shell and grain.

leave hollow shells. Grains up to about 15 m, form a thicker layer of C–S–H, but still have a small hollow centre. The probability of intersecting one of these small hollow centres in a 2D section is low, so they are rarely seen in polished sections (however, one can be seen in the bottom left corner of Fig. 4(a)). For grains larger than about 15 μm the gap will be completely infilled by C–S–H, leaving an anhydrous core surrounded by a layer of C–S–H.

5. Inner, outer and undifferentiated product

Various proposals have been made regarding the nomenclature of the different types of C–S–H presented above. Visually there is a clear difference between the diffuse product that forms the first hydrate shells and the more homogeneous product that forms the major part of the rims around the unhydrated cement cores in the larger grains. The terminology of outer, for the former and inner for the latter is probably the most widely accepted. As the exact position of the first C–S–H rim with respect to the original grain surface is not known, there is some debate as to the precision of these terms, but any discrepancy is only a few tenths of a micron at most, so for simplicity the terminology "outer"/"inner" is preferred. Jennings [3] has proposed two types of C–S–H, termed low density and high density, based on their accessibility to nitrogen and these probably correspond broadly to the outer and inner products seen in BSE images.

It is important to note that large areas of the microstructure seen on 2D sections cannot be clearly distinguished as belonging to any particular grain (see for example Figs. 3–5). This arises partly because there are a large number of small grains and partly because 2D sections often pass through the outer edges of cement grain hydration products. Such areas have been termed undesignated product [4] or groundmass [5]. Comparison of images at 1 day (Fig. 8) and considerably later ages (e.g. Figs. 3 and 4) indicates that there is considerable infilling of the large capillary pores by this undifferentiated product over the first month or so of hydration.

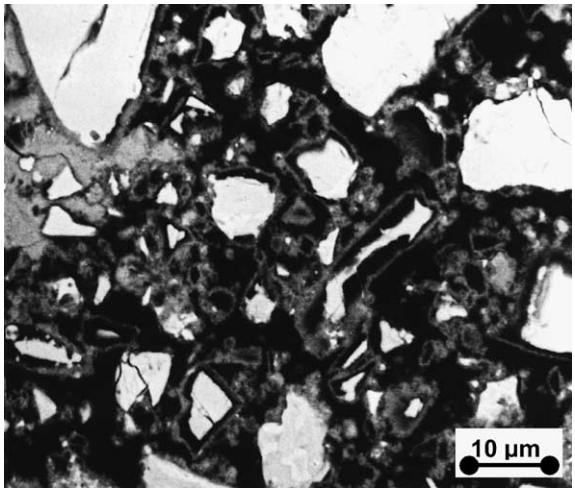

Fig. 8. BSE image of paste ($w/c = 0.5$) hydrated for 1 day. Separated hydration shells can be seen around almost all the grains. At this stage there is a large amount of pore space.

6. Aluminate containing phases

The hydration of C_3A (and perhaps Fss) leads to the formation of hydration products containing alumina. At early ages when ample sulfate is available ettringite or AFt phase is formed, this has a morphology of thin hexagonal needles less than a micron across. Despite the small size of the crystals, they may be observed in young pastes (Fig. 9). Comparison with a secondary electron image of a fracture surface (Fig. 10) clearly demonstrates the difference in resolution of the two techniques.

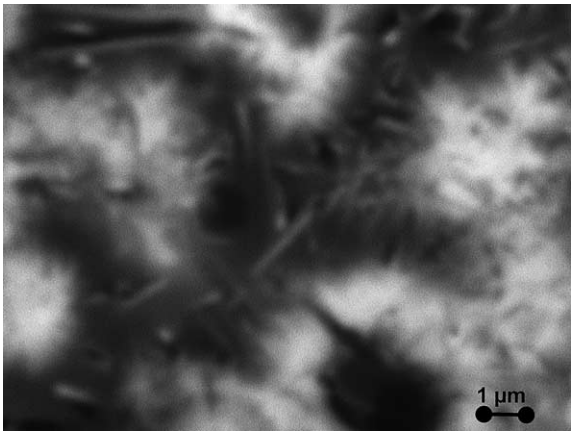

Fig. 9. High magnification view of polished, resin impregnated paste, showing ettringite needles mixed with the C–S–H and protruding into the pore space.

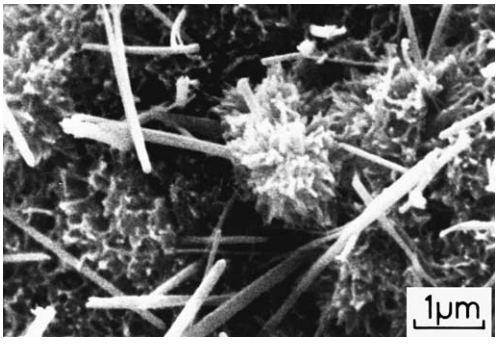

Fig. 10. Secondary electron view of a fracture surface, showing the same features as Fig. 10. This also illustrates the difference in resolution between BSE images of polished sections and secondary images of fracture surfaces.

At later ages, if further C_3A is available ettringite may react with this phase to give monosulfate:

$$2C_3A + C_3A \cdot 3C\bar{S} \cdot H_{32} + 4H \Rightarrow 3C_3A \cdot C\bar{S} \cdot H_{12}$$

As this only forms in the presence of C_3A it is typical to find small compact crystals replacing small cement grains (Fig. 11). However, considerable monosulfate also exists as fine crystals intermixed with the C–S–H.

It is also quite normal for ettringite to persist in old pastes, but it is usually difficult to identify individual crystals as these become intermixed with C–S–H. Under some conditions, this fine ettringite may recrystallise in pores and voids, where it is visible as large masses. A similar situation arises in concrete cured at elevated temperatures, where ettringite does not form during the initial hydration, but will do so later, in the presence of moisture, when the concrete returns to ambient temperatures. Fig. 12 shows a section of mortar cured at elevated temperature (90 °C, 12 h) and then stored in water for 200 days at 20 °C. The masses of ettringite which have formed are indicated. When ettringite is present in this form it may be difficult to differentiate from monosulfate by morphology alone. Microanalysis is necessary to distinguish between the two phases.

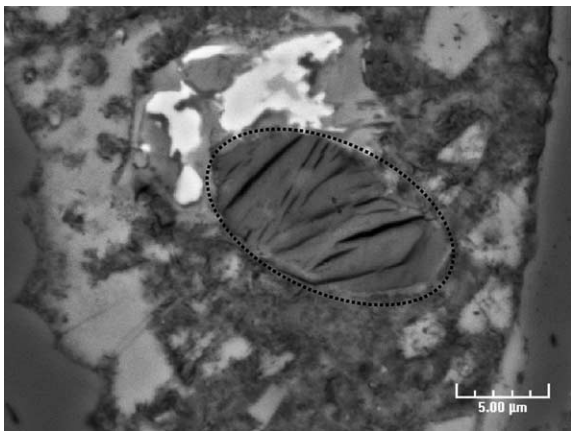

Fig. 11. Mature paste showing mass of monsulfate, circled. The cracks (probably formed on drying) lie along the {001} cleavage planes of the platy hexagonal crystals.

When phases are finely intermixed, their presence can still be deduced by making many microanalyses and plotting them on graphs such as Fig. 13. This shows

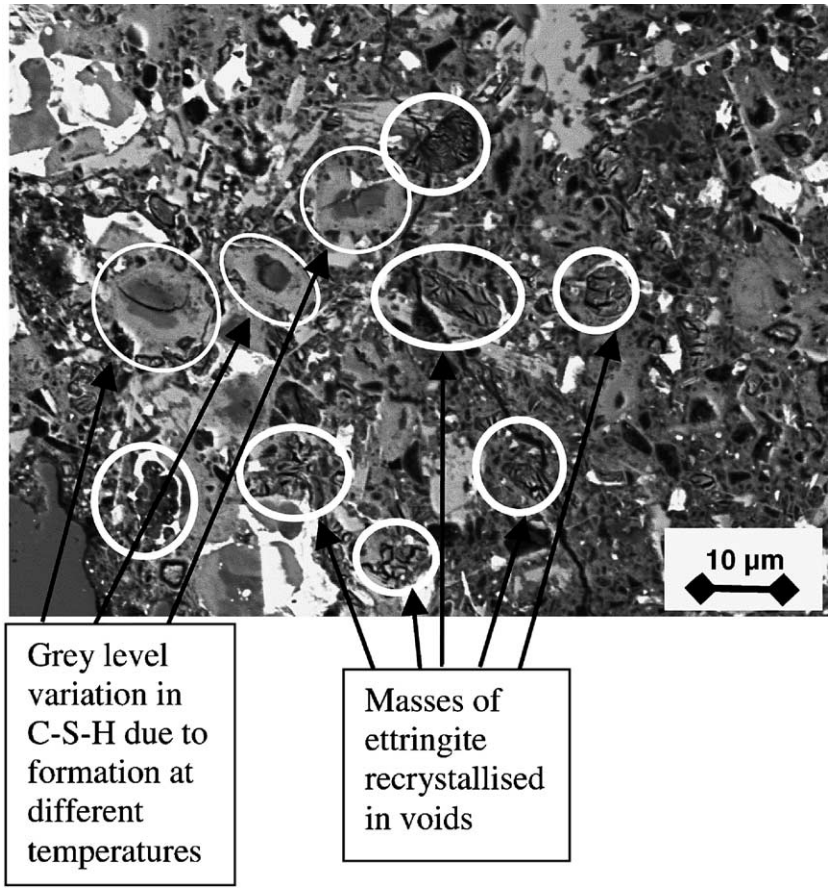

Fig. 12. Mortar cured at 90 °C for 12 h and then stored in water at 20 °C for 200 days. This microstructure exhibits "delayed" ettringite, which has formed in the hardened structure as large masses filling voids. However, it should be noted that this mortar showed no expansion on storage. The second feature is the two tone grain relics, containing bright inner C–S–H formed at the high temperature with darker inner product at the centre, formed at 20 °C during subsequent water storage.

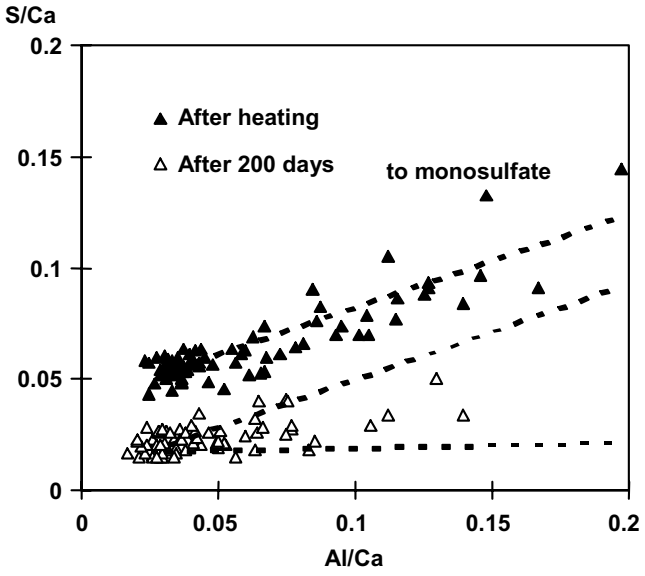

Fig. 13. Example of graphical treatment of microanalyses. Due to the large interaction volume each analysis points relates to a volume of about 1–2 μm across, which will usually contain a mixture of phases. To understand the mixtures present and to deal with the statistical variations of composition plots such as that shown enable the trends in the atom ratios to be seen. In the example of a heat treated paste the microanalysis points indicate a C–S–H with a relatively high content of absorbed sulfate after heat treatment mixed with fine calcium alumino monosulfate. During water storage the sulfate content of the C–S–H decreases.

points analysed in the undifferentiated product for mortars heat cured at 90 °C, immediately after curing and then again after 200 days immersion in water at room temperature. Immediately after curing the cluster of points on the left correspond to C–S–H containing absorbed sulfate ions, the points extending along the dotted line to the upper right correspond to mixtures of this C–S–H with calcium alumino monosulfate. After storage for 200 days in water the absorbed C–S–H contains much less absorbed sulfate and the dispersed points indicate that the intermixed phases are also low in sulfate. Such analyses have been used to understand the processes which occasionally lead to expansion of materials which have been exposed to elevated temperatures during curing [6,7].

7. Grey level variations in C–S–H

A subject of some discussion is the variations in the grey level that may be observed in C–S–H phase [8–10]. The C–S–H phase is a product of variable composition, particularly in terms of the ratio of calcium oxide to silica (C/S). Variations may also occur in the degree of microporosity. Both these factors affect the grey level in BSE images.

Variations in C/S ratio occur when the activity of calcium in the surrounding solution changes. This occurs when calcium is leached from the cement paste, when carbonation occurs, and also when there is a large amount of pozzolanic reaction, such as may occur in pastes containing silica fume. C–S–H with lower C/S ratio is darker in BSE images than that with higher C/S ratio.

Variations in microporosity have been found to occur when the C–S–H forms at different temperatures, higher temperatures lead to "denser" C–S–H with lower microporosity and so a lighter appearance in BSE images. In pastes cured at elevated temperatures and then stored in water at room temperatures, two distinct C–S–Hs may be observed in the relics of the larger cement grains, as indicated in Fig. 12. The outermost, bright layer formed first at high temperature and the innermost dark layer formed at room temperature. Interestingly the grey level of the C–S–H formed at room temperature is darker than in an equivalent paste cured continuously at room temperature, the reasons for this difference are not well understood.

When the circumstances leading to grey level variation are not known, the two effects may be distinguished by combining BSE imaging with microanalyses as described above [10].

8. Quantification

The features described so far can be found in pastes of any Portland cement. Therefore in order to be able to differentiate between pastes and ultimately in order to build structure–property relationships, it is highly desirable to be able to quantify the microstructural features. The reproducible contrast of backscattered electron images makes them well suited for this. As discussed in Section 1, BSE images only show two-dimensional sections. The only measure which can be translated directly from 2D to 3D is the overall area fraction, which is directly equivalent to the volume fraction. For most features, such as porosity, it is not possible to derive quantitative 3D size distributions from data obtained from 2D sections, much less to draw conclusions about connectivity.

A typical grey level histogram of a mature cement paste is shown in Fig. 14. The peak on the right, corresponding to the anhydrous (unreacted) cement is well distinguished and it is comparatively easy to separate out this phase by "thresholding" the image at the minimum in the histogram.

As cement is a heterogeneous material, several fields must be measured to obtain a result which is representative of the specimen as a whole. The higher the magnification, the more fields must be analysed to cover the same total area. This results is a trade-off between the better resolution which can be obtained at higher magnification and the larger area measured at lower magnifications. Statistically, the advantage of analysing

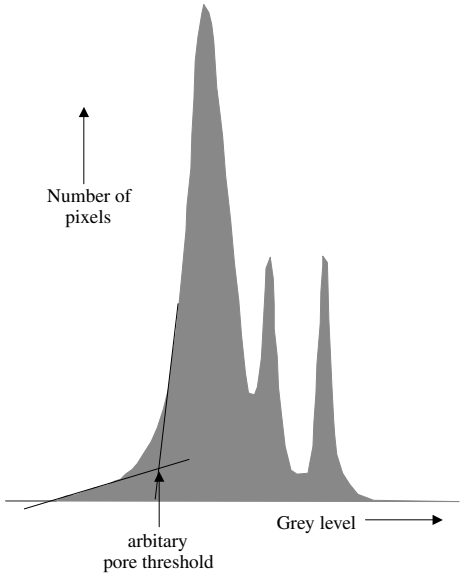

Fig. 14. Typical grey level histogram of hardened cement paste. From the right (highest grey levels) the peaks correspond to anhydrous material, calcium hydroxide and C–S–H respectively. There is no discrete peak for the porosity as discussed in the text.

larger areas (low magnification) outweighs the gain in resolution at higher magnifications (as summed up in the phrase "*Do more less well*"). Scrivener et al. [11] found that for a cement paste analysis of ten fields at 400× was sufficient to give a standard error of around 0.6%. More recently, Mouret et al. [12] have applied a more rigorous statistical analysis to show that a magnification of 200× is sufficient to give good results for the anhydrous phase and that measurement of 30 images give a mean with an error of <0.2% in pastes and mortars. Studies have shown that the amount of unreacted cement measured in this way corresponds well with independent measures of hydration [11,13].

Although the peak corresponding to calcium hydroxide is relatively well defined in histograms of well polished sections, the complex interpenetrations of this phase with other phases in the microstructure, means that the results of measurement by image analysis on BSE images are less reliable than results obtained by more traditional techniques, such as thermogravimetric analysis (TGA) or X-ray diffraction (XRD) [12,13]. Nevertheless, the possibility to measure local differences in the relative amounts between different areas of the microstructure are a great advantage, for example in studies of the ITZ described below.

The remaining thresholding of BSE images is that between the pores and other hydration products (as discussed above the resolution and grey level differences between the different hydration products (C–S–H, ettringite, monosulfate, etc.) are too small for these to be individually distinguished by image analysis). As seen in the histogram (Fig. 14) there is no separate peak for pores in pastes more than a few days old. This is partly due to the resolution of the BSE technique and partly to the physical nature of the pore boundary. Although the drying and preparation of the specimens for examination in the SEM undoubtedly alters the C–S–H structure, these changes are of most significance at a scale below the resolution of BSE images.

At high magnifications (e.g. Fig. 9), the rough, diffuse character of the C–S–H surface can be seen, corresponding to the "sea urchin" morphology, familiar in secondary images of fracture surfaces (Fig. 10). In mature pastes, most pores are below a few microns in size, so some BSEs will be scattered from the sides of the pores or bottom. Because of these effects, it is not possible to define an unambiguous boundary between pores and C–S–H and any threshold must be fixed in an arbitrary way. Several strategies have been elaborated to make this threshold reproducible, which is the essential criterion for making comparative measures between specimens. One such strategy, adopted in the work of Patel, is shown in Fig. 14. No claim is made for this being necessarily the best, but this method has been rigorously compared with independent measures of porosity over a wide range of water to cement ratios and cement types (Fig. 15). When such a strategy is used it is not really correct to talk about a minimum pores size being measured. Some areas, which in fact contain solid intermixed which small pores, are defined as pores and some areas in which the ratio of solid to pores is somewhat higher are defined as solid. This is why reasonable correlation with other measures of porosity can be obtained (as described below) even though the min-

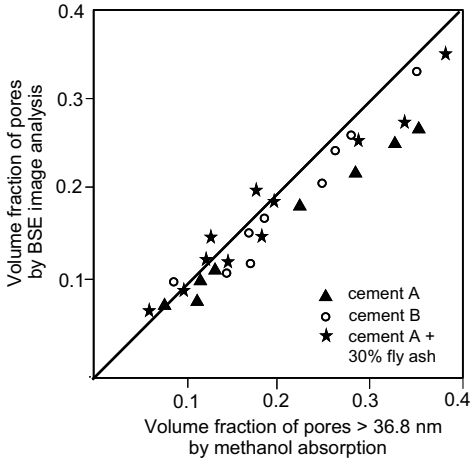

Fig. 15. Correlation of pores measured by two independent techniques—image analysis (IA) and methanol absorption (MA). The points cover three different cementitious types at 3 w/c ratios and at 3 ages. The solid line shows the 1:1 correspondence, not the best fit. At high levels of porosity the IA technique underestimates the porosity, but at lower levels of porosity the agreement is quite good. Adapted from Ref. [13].

imum size of pores resolved by such methods is well below the resolution of the BSE images.

In the studies of Patel [11,13] measurements of pores >36.8 nm were compared with the porosity measured by BSE image analysis. The specimens were first dried by solvent exchange of the water with methanol, and then the methanol was removed by evaporation. The dried specimens were placed over methanol in a desiccator alongside samples of porous glass of defined pore size of 36.8 nm. The cement and glass specimens were regularly weighed. The weight gain curve of the glass, due to progressive methanol absorption, shows a sharp break at the point when all the 36.8 nm pores are filled. The weight gain of the cement samples at the same time is then used to calculate the volume of pores below 36.8 nm in size and the volume of pores above this size calculated by difference from the total porosity. Fig. 15 shows the comparison of the pores greater than 36.8 nm measured by the methanol absorption method and the pores measured by image analysis for three cementitious types each at three w/c ratios, each at three ages. The correlation between the two measures is reasonable, although at high porosities the values obtained by image analysis appear to be lower than those obtained by methanol absorption. It is clear that comparative measures of porosity between different cement pastes, or between different areas within a paste can be made.

As described by Diamond [14] there is a dramatic difference of at least an order of magnitude between the apparent pore sizes measured by mercury intrusion porosimetry and that seen in BSE images. This can be mainly attributed to the fact that MIP measures the pore entry radius, The access to large regions of porosity may be controlled by an entry of very small size and all the pores in this region (whatever their actual size) will be assigned to the size of the small entry.

9. Interfacial transition zone

Throughout this paper the term ''cement paste'' has been used synonymously for the cement paste component in mortar and concrete. In fact it is in these two latter forms that cement is used and in a few important respects their microstructure differs significantly from that of plain cement paste. First the aggregate particles add a new level of heterogeneity and secondly they disrupt the packing of cement particles locally at the cement paste aggregate interface creating an interfacial transition zone (ITZ) [15–17].

The large aggregate particles disrupt the random packing of the cement grains to give a zone adjacent to the interface which has a deficit of cement grains. The size of this zone is commensurate with that of the cement grains, with the most significant differences occurring over the first 15–20 μm from the interface. In an image such as Fig. 16, this 15–20 μm zone (indicated by the white line) appears to be minor compared to the bulk paste, but it in fact makes up some 20–30% of the total paste volume in a typical concrete. The deficit of cement grains in the ITZ means that initially there is effectively a higher water to cement ratio in this region, so for a given overall water to cement ratio the water to the cement ratio of the ''bulk'' cement paste is correspondingly lower.

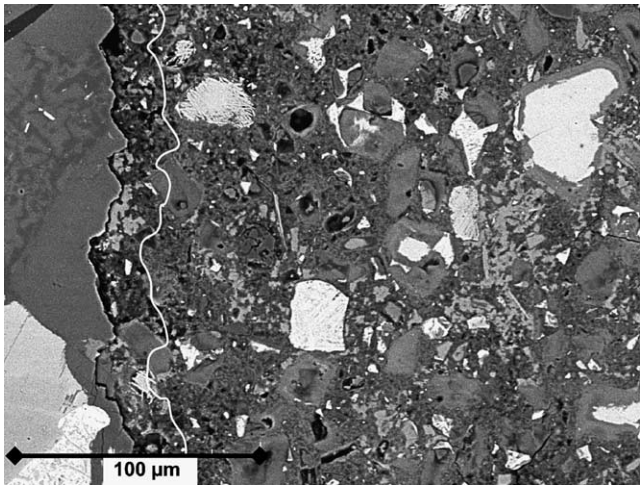

Fig. 16. BSE image of concrete including paste aggregate interface. The so-called interfacial transition zone is not a separate region but a gradual transition from the aggregate surface into the ''bulk'' paste. The most significant differences, due to the perturbed packing of the cement grains, occur in the first 15–20 μm—comparable with the average size of the cement grains. As shown in this image, by the white line, this zone appears very small, but it may constitute 20–30% of the paste in a concrete.

The high degree of heterogeneity introduced by the aggregate particles and the relative movement of paste and aggregate during mixing of the concrete mean that there are large variations in the microstructure of the ITZ. This is illustrated in Fig. 17, which shows a region where several cement grains are clustered together and there are marked differences in the paste density. In addition, large deposits of calcium hydroxide can be seen along some aggregate surfaces, while others have very little calcium hydroxide in their vicinity. These variations make it very difficult to characterise the ''average'' ITZ microstructure. However, quantification has been made of the relative amounts of anhydrous cement, calcium hydroxide, other hydration products and pores in bands equidistant from the aggregate surfaces, over a large number of images taken on different aggregate particles throughout a concrete. From this the proportions of the different microstructural components in the ''average'' ITZ can be measured as shown in Fig. 18 for a 28 day old concrete of nominal water to cement ration 0.4.

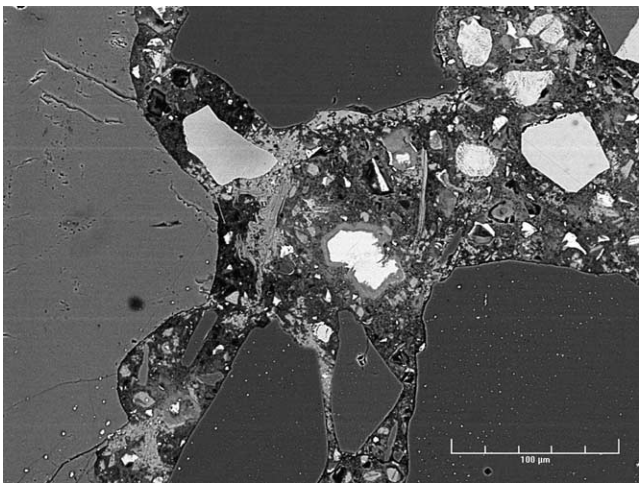

Fig. 17. BSE image of concrete showing heterogeneity of structure. The paste between the aggregate grains in the top left of the image is significantly less dense. Deposits of calcium hydroxide are fairly extensive at some interfaces, while absent at others. In order to quantify the "average" structure many different images must be measured.

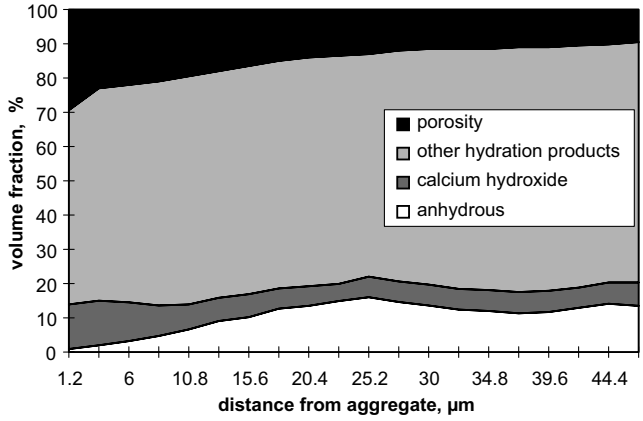

Fig. 18. "Average" distribution of microstructural constituents in the interfacial transition zone of a 28 day old concrete. Adapted from Ref. [17].

10. Analysis of degradation processes

BSE imaging provides a powerful tool for studying degradation processes. It is comparatively easy to prepare sections cut perpendicular to an exposed surface and so study the depth of alteration at the microscopic level. The changes which occur vary widely with the exposure conditions, length of exposure and nature of the concrete. It is only possible to show one example here of a concrete subject to natural weathering in the climate of Northern Europe for several years (Fig. 19). Several hundred microns have been eroded from the original surface by the action of rain (which is acidic relative to concrete) and by freeze thaw scaling. A layer of paste about 100 μm thick, now at the surface, appears much darker because all the calcium has been leached from it. Below this is another 100 μm layer of carbonated concrete in which the anhydrous cement cores have reacted to silica gel. Below this is the more or less unweathered concrete.

The ability to observe degradation on such a fine scale should enable more reliable extrapolation of results from short-term tests to estimation of service life. This can be achieved by verifying the relevance of accelerated test methods to field situations, by enabling the degradation mechanisms to be understood, and by enabling models to be calibrated. It is hoped that such applications which will be developed in the future.

11. Concluding remarks

This paper aimed to give the reader some insights into the use of backscattered electron imaging for the study of cement and concrete. Over the last 20 years, the potential of the techniques to reveal the microstructure of representative sections has been applied to a wide variety of studies, of which it has only been possible to

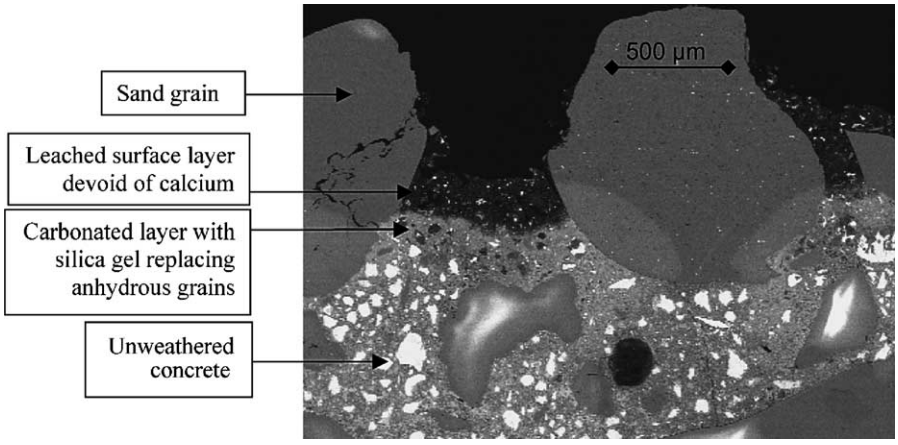

Fig. 19. Example of use of BSE imaging in the study of durability. This concrete was exposed for 10 years in a wet cold climate. The section was cut perpendicular to the surface. The outer surface has been eroded. Below this eroded surface there is a severely leached layer, followed by a carbonated layer.

present a few illustrative examples, but they have hopefully shown the potential of the BSE to study:

- the microstructure of cement hydration, including the differentiation of the anhydrous components, the major hydration products and pore spaces
- the development of microstructure associated with atypical hydration processes, e.g. high temperature curing, and degradation process, e.g. leaching
- the differences in microstructure between cement paste produced in isolation and cement paste which is part of a cement or mortar, and in particular the interfacial transition zone ITZ.

The author believes that the challenge for the future lies in moving towards studies which place more emphasis on the quantitative potential of BSE, rather than the qualitative characterisation which currently dominates. One of the biggest obstacles to this is time and the lack of dedicated equipment. There is a large difference in the amount of time needed to acquire a few illustrative images and that needed to acquire the 30–100+ images which may be needed to derive quantitative information. The fact that most SEM facilities are often shared, with each user only being allocated a few hour at a time impedes the more widespread use of systematic methods.

Acknowledgements

The author would like to acknowledge several people who have contributed to the view of concrete microstructure presented here. The PhD studies of Hitesh Patel and Alison Crumbie allowed us make significant progress towards obtaining quantitative measures of concrete microstructures. The theses of Mathew Lewis and Charlotte Famy allowed us to study the effect of elevated temperatures on cement paste microstructures. Finally I would like to acknowledge the huge influence of many conversations with the late Hal Taylor, who followed closely much of the work presented here.

References

[1] Scrivener KL, Pratt PL. Characterisation of Portland cement hydration by electron optical techniques. In: Electron microscopy of materials. Proc Mat Res Soc Symp 1983, vol. 31. p. 351–6.
[2] Scrivener KL, Pratt PL. Backscattered electron images of polished cement sections in the scanning electron microscope. In: Proc Sixth Int Conf Cement Microscopy, Albuquerque, 1984. p. 145–55.
[3] Tennis P, Jennings HM. A model for two types of calcium silicate hydrate in the microstructure of Portland cement pastes. Cem Concr Res 2000;30:855–63.
[4] Taylor HFW. Cement chemistry. 2nd ed. London: Thomas Telford; 1997.
[5] Diamond S, Bonen D. A re-evaluation of hardened cement paste microstructure based on backscatter SEM investigations. In: Diamond S, Mindess S, Glasser FP, Roberts LW, Skalny JP, Wakeley LD, editors. Microstructure of cement based systems/bonding and interfaces in cementitious materials. Materials Research Society Symposium Proceedings, 1995, vol. 370. p. 13–22.
[6] Scrivener KL, Lewis MC. Microstructural and microanalytical study of heat cured mortars and delayed ettringite formation. Paper 4iv062, Proc 10th ICCC, Göteborg, 1997.
[7] Famy C, Scrivener KL, Brough AR, Atkinson A, Lachowski E. Characterisation of C–S–H products in expansive and non-expansive heat-cured mortars: an electron microscopy study. Proceeding of the 5th CANMET/ACI International Conference of Concrete Durability, Barcelona, Spain, 20001, vol. 1. p. 385–402.
[8] Scrivener KL. The effect of heat treatment on inner product C–S–H. Cem Concr Res 1992;22:1224–6.
[9] Diamond S, Olek J, Wang Y. The occurrence of two-tone structures in room temperature cured cement pastes. Cem Concr Res 1998;28:1237–43.
[10] Famy C, Scrivener KL, Crumbie AK. What causes differences of C–S–H gel grey levels in backscattered electron images? Cem Concr Res 2002;32(9):1465–71.
[11] Scrivener KL, Patel HH, Pratt PL, Parrott LJ. Analysis of phases in cement paste using backscattered electron images, methanol adsorption and thermogravimetric analysis. In: Microstructural Development During the Hydration of Cement. Proc Mat Res Soc Symp 1987, vol. 85. p. 67–76.
[12] Mouret M, Ringot E, Bascoul A. Image analysis: A tool for the characterisation of cement in concrete—metrological aspects of magnification on measurement. Cem Concr Comp 2001;23:201–6.
[13] Patel HH. PhD Thesis. London, University of London, 1987.
[14] Diamond S. Mercury porosimetry: an inappropriate method for the measurement of pore size distributions in cement-based materials. Cem Concr Res 2000;30:1517–25.
[15] Scrivener KL, Pratt P. Characterisation of interfacial microstructures. In: Maso JC, editor. Interfacial transition zone in concrete, State of the Art Report, RILEM Committee 108 ICC. London, F.N. Spon, 1996. p. 3–17.
[16] Scrivener KL. Characterisation of the ITZ and its quantification by test methods. State of the Art Report, RILEM Committee TC-ETZ, 1999.
[17] Crumbie AK. PhD thesis. London, University of London, 1994.